Role of metabolic pathways and sensors in regulation of dendritic cell-driven T cell responses

Pelgrom, L.R.

7

Protein O-GlcNAcylation and low glycolysis underpin Th2 polarization by dendritic cells

Leonard R. Pelgrom
Alexey A. Sergushichev
Marjolein Quik
Alwin J. van der Ham
Lisa W. Bloemberg
Beatrice M. F. Winkel
Gabriele Schramm
Cornelis H. Hokke
Meta Roestenberg
Maxim N. Artyomov
Bart Everts

Manuscript in preparation

Abstract

Activation of dendritic cells (DCs) for priming of T cell responses is dependent on rewiring of their cellular metabolism. However, the metabolic characteristics of and requirements for DCs to prime T helper 2 (Th2) responses are unknown. Using unbiased transcriptomics and non-targeted metabolomics we show here that helminth antigen-conditioned human DCs with the ability to drive Th2 polarization can be distinguished from unstimulated DCs and other Th-priming DCs by a unique metabolic signature of suppressed glycolytic activity, and elevated abundance of hexosamine biosynthesis pathway metabolites including UDP-GlcNAc which is the key substrate of O-GlcNAcylation, a post-translational modification of intracellular proteins. This metabolic reprogramming is functionally important specifically for priming of Th2 responses as suppression of glycolysis was sufficient to condition DCs for Th2 polarization. Furthermore, inhibition of O-GlcNAcylation in DCs impaired their ability to drive Th2, but not Th1 or Th17 responses. These findings were corroborated in experiments with DCs stimulated with allergens. Finally, a controlled human infection trial with the parasitic hookworm *Necator americanus* revealed a consistent increase in intracellular O-GlcNAcylation in circulating CD1c+ type 2 conventional DCs, but not in CD141+ cDC1s and CD123+ pDCs, providing credence for relevance of this pathway in humans. In summary, we uncovered a unique metabolic program in DCs selectively required for Th2 polarization which may aid in the development of therapeutic strategies aimed at modulating type 2 immunity.

Introduction

Type 2 immune responses are crucial for controlling parasitic helminth infections and mediating tissue repair. Additionally, they can confer protection against development of type 2 diabetes and atherosclerosis which is a major cause of cardiovascular disease. However, overzealous type 2 immunity can lead to allergies and support tumor growth [1]. This growing evidence of type 2 immunity's crucial role in the development and outcome of several important diseases signifies the importance of better understanding how they are initiated.

Dendritic cells (DCs) are the quintessential antigen presenting cell of the innate immune system. Antigen presentation and costimulatory signals provided by DCs allow them to induce T cell activation. Additionally, polarizing cytokines secreted by DCs instruct T cells to undergo specific differentiation programs [2]. As such, they play a key role in the initiation and regulation of type 2 immune responses by governing the priming and polarization of T helper (Th) 2 responses. The importance of DCs in type 2 immune responses indicates the need for better understanding of the mechanisms through which DCs initiate these responses, which could aid the development of novel therapeutic interventions for diseases in which type 2 immune responses are involved.

There is a longstanding interest in delineating signals, i.e. cytokines and membrane-bound proteins, expressed by DCs that instruct Th cells to initiate a certain differentiation program. These polarizing signals have been extensively characterized in the context of priming of Th1, Th17 and regulatory T (Treg) cell responses. However, for Th2-priming DCs these remain poorly defined. In part this stems from the fact that Th2-priming DCs do not appear to secrete polarizing cytokines analogous to IL-12, IL-23, or TGFβ that contribute to Th1, Th17 or Treg differentiation, respectively [3, 4].

Apart from studying immunological features to understand how DCs function, there is a growing appreciation that cellular metabolism plays a central role in regulation of DC biology [5, 6]. It is now clear that activation and their ability to prime T cell responses is accompanied by and underpinned by specific metabolic reprogramming [7]. Activation, migration, and production of pro-inflammatory cytokine production of DCs is dependent on aerobic glycolysis [8-11]. Moreover, evidence is emerging that the unique immunological signatures that differentiate DCs with different Th cell-priming capacities are paralleled and supported by distinct metabolic signatures [7]. The production of the Th1-priming cytokine interleukin (IL)-12 [8, 10, 11] and Th17-priming IL-6 are dependent on glycolysis [12]. The conditioning of human monocyte-derived DCs (moDCs) for a tolerogenic phenotype is also dependent on glycolysis [13,

14], either independently from [13] or coupled to high mitochondrial respiration [14], depending on the tolerogenic compounds used. Likewise, DCs that were rendered tolerogenic by the tumor microenvironment *in vivo*, relied on fatty acid oxidation for their ability to promote Treg responses [15]. On the other hand, the metabolic properties of Th2-priming DCs and the metabolic programs that support their ability to prime a Th2 response are still poorly defined. Thus far, the best metabolic description of DCs that can potentially prime Th2 cells comes from a recent study comparing the metabolism of *in vitro*-cultured murine DCs after conditioning with strong and weak stimuli [9]. In this study, stimulation with allergenic house dust mite led to an early induction of glycolysis, as did stimulation with bacterial lipopolysaccharides or yeast β-glucans that were depleted of their toll-like receptor (TLR) ligands (= tolerogenic DC associated). There were differences however in the metabolic signaling pathways associated and the duration of glycolytic reprogramming. Nevertheless, the T cell-priming capacity of these DCs and their dependence on unique metabolic states was not evaluated [9].

Therefore, in the present study, we set out to characterize the metabolic properties of Th2-priming DCs and define which metabolic programs license these cells for Th2 polarization. To this end, we used the combined experimental and computational pipeline of concordant metabolomics integration with transcription (CoMBI-T), previously applied in macrophages [16], to define the metabolic signature of human DCs conditioned to prime Th2 responses and to compare that to those of Th1- and Th17-priming DCs. We found that Th2-priming DCs can be distinguished from Th1- and Th17-priming DCs by their reduced glycolytic potential; a metabolic feature that in itself was sufficient to condition DCs for Th2 priming. Moreover, these Th2-priming DCs displayed a distinct metabolic signature of UDP-GlcNAc synthesis and O-GlcNAc transferase (OGT) enzyme expression. Blocking protein O-GlcNAcylation, either pharmacologically or genetically, selectively reduced the Th2-priming capacity of these DCs. Together, these findings define low glycolysis and protein O-GlcNAcylation as unique metabolic requirements for Th2 polarization by DCs. These requirements may be amenable for modulation in therapeutic settings to shape type 2 immune responses.

Results

Inhibition of glycolysis in DCs is associated with Th2 priming

As a model to study the metabolic properties of and requirements for Th2 polarization by DCs, we used the schistosome-derived glycoprotein omega-1 to condition moDCs for Th2 priming (Th2-DCs). Omega-1 is a well-studied and potent inducer of Th2 responses both *in vitro* and *in vivo* [17-19]. The

transcriptome of these Th2-DCs was compared to those of unstimulated (iDCs), LPS+PolyIC-stimulated Th1-priming (Th1-DCs) and zymosan-stimulated Th17-priming DCs (Th17-DCs; Figure 1A-B and S1A-B). As previously reported, Th2-DCs did not display a strong upregulation of costimulatory molecules nor cytokine production, unlike Th1- and Th17- DCs (Figure S1C-F & [20]). In line with this muted activation profile, the transcriptome of Th2-DCs did not differ as much from iDCs as the transcriptomes of Th1-DCs and Th17-DCs. Nevertheless, the overall transcriptome of Th2-DCs was clearly distinct from iDCs (Figure 1C). Next, we generated transcriptional clusters with genes related to cellular metabolism that can be used to distinguish these DCs with distinct Th-priming capacities (Figure 1D). Pathway analysis was performed on overrepresented genes within those clusters to elucidate which metabolic pathways best represent these clusters. This analysis uncovered 4 metabolic clusters - in which genes related to glycolysis (Cluster 3), citrate metabolism (Cluster 8), glycerophospholipid metabolism (Cluster 9) and gonadotropin-releasing hormone (Cluster 11) were most significantly overrepresented - that could differentiate Th2-DCs from iDCs (Figure 1D). Of these clusters, only glycolysis (Figure 1E and S2A) and glycerophospholipid metabolism could be used to additionally distinguish Th2-DCs from Th1-DCs and Th17-DCs.

To establish the biological relevance of these findings we analyzed the glycolytic flux in differently conditioned DCs. Baseline rates of glycolysis were not significantly lower in Th2-DCs compared to iDCs as determined by extracellular flux (XF) analysis (Figure 1F) and lactate release (Figure 1G). Nonetheless, maximal glycolytic capacity (Figure 1F) and LPS-induced glycolytic reprogramming were impaired in Th2-DCs (Figure 1H-I). In contrast, Th1-DCs and Th17-DCs displayed strongly increased glycolytic rates, glycolytic capacity, and lactate release (Figure 1G). Th2-DCs did not compensate for a lower glycolytic flux by heightening the production of ATP through oxidative phosphorylation. In fact, consistent with the reduced expression of genes involved in TCA cycle metabolism (Figure S2B-C), Th2-DCs displayed the lowest mitochondrial respiratory activity of all DCs, both in terms of baseline and maximal respiration as well as oxygen consumption linked to ATP synthesis (Figure S3). This observation indicates a low overall bioenergetic status of Th2-DCs.

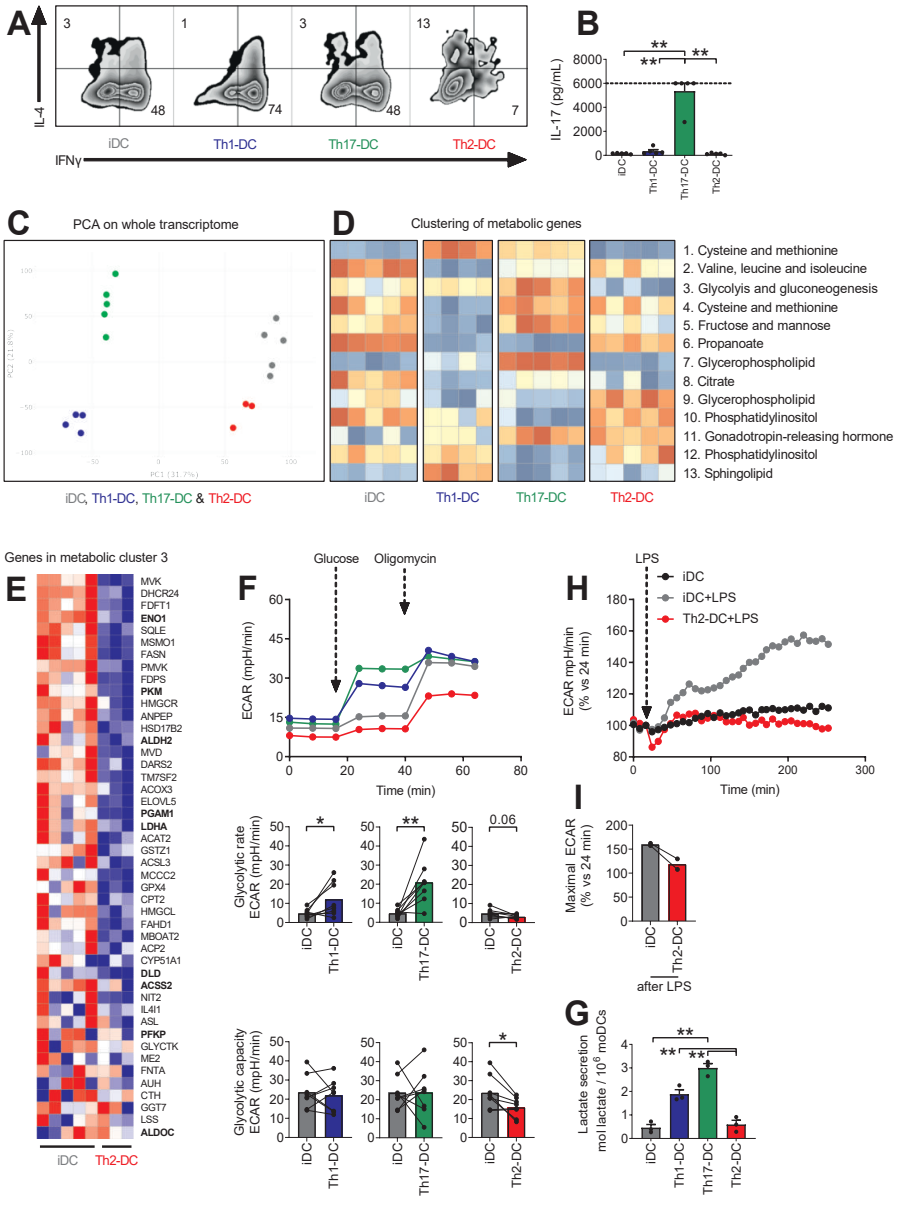
A
IL-4
IFNγ
3
48
1
74
3
48
13
7
iDC
Th1-DC
Th17-DC
Th2-DC
B
IL-17 (pg/mL)
8000
6000
4000
2000
0
**
**
**
C
PCA on whole transcriptome
iDC, Th1-DC, Th17-DC & Th2-DC
D
Clustering of metabolic genes
iDC
Th1-DC
Th17-DC
Th2-DC
1. Cysteine and methionine
2. Valine, leucine and isoleucine
3. Glycolysis and gluconeogenesis
4. Cysteine and methionine
5. Fructose and mannose
6. Propanoate
7. Glycerophospholipid
8. Citrate
9. Glycerophospholipid
10. Phosphatidylinositol
11. Gonadotropin-releasing hormone
12. Phosphatidylinositol
13. Sphingolipid
Genes in metabolic cluster 3
E
MVK
DHCR24
FDFT1
ENO1
SQLE
MSMO1
FASN
PMVK
FDPS
PKM
HMGCR
ANPEP
HSD17B2
ALDH2
MVD
DARS2
TM7SF2
ACOX3
ELOVL5
PGAM1
LDHA
ACAT2
GSTZ1
ACSL3
MCCC2
GPX4
CPT2
HMGCL
FAHD1
MBOAT2
ACP2
CYP51A1
DLD
ACSS2
NIT2
IL4I1
ASL
PFKP
GLYCTK
ME2
FNTA
AUH
CTH
GGT7
LSS
ALDOC
iDC
Th2-DC
F
Glucose
Oligomycin
ECAR (mpH/min)
Time (min)
Glycolytic rate ECAR (mpH/min)
Glycolytic capacity ECAR (mpH/min)
*
**
0.06
*
iDC
Th1-DC
Th17-DC
Th2-DC
H
LPS
iDC
iDC+LPS
Th2-DC+LPS
ECAR mpH/min (% vs 24 min)
Time (min)
I
Maximal ECAR (% vs 24 min)
after LPS
G
Lactate secretion mol lactate / 10^6 moDCs
**
**
**

Figure 1. Inhibition of glycolysis in DCs is associated with Th2 priming.

Human moDCs were left untreated (iDC in grey) or stimulated for 24h with either LPS+PolyIC (Th1-DC in dark blue), zymosan (Th17-DC in green) or omega-1 (Th2-DC in red). Supernatants were then collected for determination of extracellular lactate (F) and DCs were set aside for either co-culture with allogeneic T cells (A-B), RNA-sequencing (C-E) and measurements of glycolysis using extracellular flux (XF) analysis (F, H-I).
(A) Representative histograms of T cell intracellular IFNγ and IL-4 that was analyzed by flow cytometry after a 6h stimulation with phorbol myristate acetate (PMA) and ionomycin. T cells used were naïve and the culture was 11 days.
(B) Co-culture with memory T cells. Supernatants were collected after 5 days and IL-17 concentrations was determined by ELISA.
(C) Principle component analysis on total transcriptome of differently conditioned DCs.
(D) Metabolic genes were selected out of the total transcriptome of differently conditioned DCs and used to form 13 clusters with maximal distinguishing power. Different clusters with distinct combination of genes were sometimes part of the same pathway in the KEGG database (e.g. cluster 1 and 4 = cysteine and methionine metabolism).
(E) Overview of genes in metabolic cluster 3. Genes that represented more in a DC type relative to the other are in red and genes that are represented less are in blue. Genes that are part of the KEGG pathway Glycolysis / Gluconeogenesis are highlighted in bold.
(F) Glycolytic stress test in Seahorse XF analyzer which consists of sequential injections of glucose and the ATP synthase inhibitor oligomycin after which extracellular medium acidification rate (ECAR) is measured as a proxy for glycolysis-derived lactate. Glycolytic rate = the difference before and after injection of glucose. Glycolytic capacity = the difference before injection glucose and after infection of oligomycin.
(G) Lactate concentration was determined by measuring absorbance of NADH at 340 nm after the reaction of lactate with NAD by reaction with NAD by lactate dehydrogenase into pyruvate and NADH.
(H-I) Real-time changes in the ECAR of DCs treated with LPS.
The number of independent experiments is represented by symbols in the graphs and shown as mean ± SEM; *p < 0.05, **p < 0.01

Inhibition of glycolysis in DCs is sufficient for Th2 priming

This association between reduced glycolysis in Th2-DCs and their Th2-priming capacity led us to ask if lower glycolytic engagement may be functionally linked to the Th2-priming capacity of these cells. Indeed, inhibition of glycolysis using 2-deoxyglucose (2-DG) – a competitive inhibitor of hexokinase, the first enzyme in glycolysis and the first rate-limiting step of this pathway - was in itself sufficient to condition both unstimulated and LPS-activated DCs for Th2 priming (2-DG-DCs; Figure 2A-B). This observation suggests an important functional role for this type of metabolic rewiring in Th2 priming by DCs. A common characteristic of Th2-priming DCs and prerequisite for efficient Th2 priming is low IL-12 expression [17-19, 21, 22]. Indeed, 2-DG-DCs secreted little IL-12 following CD40 ligation (Figure 2C). Furthermore, 2-DG-DCs selectively displayed increased CD86 surface expression (Figure 2E), which in some contexts has been implicated as a necessary costimulatory signal by DCs to mount Th2 responses *in vivo* [23, 24]. Taken together, these data show that

lower glycolytic activity is one of the defining characteristics of Th2-priming DCs and suggest this is functionally linked to their ability to prime this Th cell response.

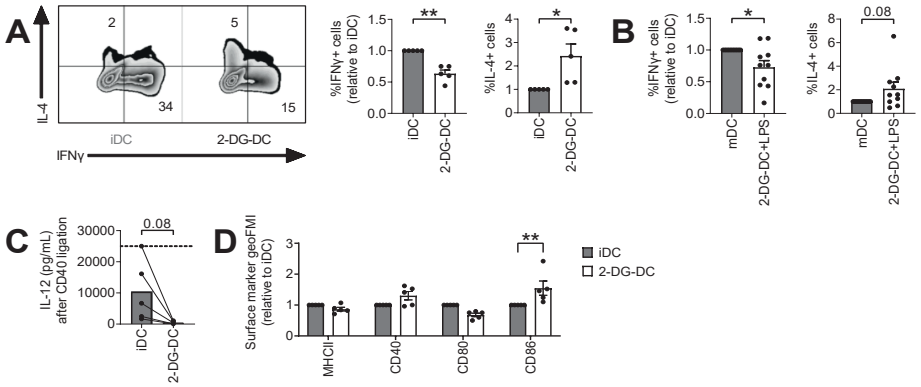

Figure 2. Inhibition of glycolysis in DCs is sufficient for Th2 priming.

Human moDCs were left untreated (iDC in grey) or stimulated for 24h with 2-deoxyglucose (2-DG-DC in white). Supernatants were then collected for determination of IL-10 secretion (D) and DCs were set aside for either co-culture with allogeneic T cells (A), determination of viability (B), IL-12p70 secretion after 24h co-culture with a CD40L expressing cell line (C) and maturation (E)
(A) On the left side, representative histograms of T cell intracellular IFNγ and IL-4 that was analyzed by flow cytometry after a 6h stimulation with phorbol myristate acetate (PMA) and ionomycin. T cells used were naïve and the culture was 11 days. On the right side, the percentages of T cells uniquely positive for either IFNγ or IL-4 are expressed relative to the iDC condition.
(B) Frequencies of dead DCs are enumerated using flow cytometry.
(C) Co-culture with CD40L expressing cell line. Supernatants were collected after 24 hours and IL-12p70 concentrations was determined by ELISA.
(D) Supernatants were collected after antigen stimulation and IL-10 concentrations was determined by ELISA.
(E) The expression of maturation makers – based on the geometric mean fluorescence – are shown relative to iDCs.
The number of independent experiments is represented by symbols in the graphs and shown as mean ± SEM; *p < 0.05, **p < 0.01

Enhanced hexosamine biosynthesis and O-GlcNAc transferase expression are unique to Th2-priming DCs

To further define and compare the metabolic characteristics of Th2-priming DCs, we additionally performed unbiased metabolomics using flow injection analysis mass spectrometry (FIA-MS) on the same cells that were used for RNA sequencing [16]. Metabolomics revealed only a handful of metabolites that significantly accumulated in Th2-DCs relative to iDCs. The majority of these are

known substrates for glycosyltransferases (Fig 3A). To improve our chances of identifying important nodes of metabolic rewiring in a non-targeted manner, we performed an integrated network analysis of transcriptional and metabolomic data using our publicly available tool (GAM; [25]).

This integrated analysis corroborated results from our initial metabolic profiling based on transcriptomic data, as it identified a suppressed glycolytic pathway as one of the main metabolic signatures of Th2-DCs in comparison to iDCs (Figure 3B). However, this analysis now additionally uncovered a significantly upregulated metabolic module of metabolic enzymes and their substrates, which are involved in the post-translational modification of intracellular proteins by transfer of GlcNAc (i.e. O-GlcNAcylation) from uridine diphosphate N-acetylglucosamine (UDP-GlcNAc). Th2-DCs were found to express increased levels of the enzymes O-GlcNAc transferase (OGT) and O-GlcNAcase (OGA; encoded by the MGEA5 gene), which attach and remove O-GlcNAc moieties from proteins, respectively (Figure 3B and S4A). Their substrate/product UDP-GlcNAc was also elevated in Th2-DCs relative to iDCs, as was its precursor N-acetyl-glucsomine-1-phosphate. Finally, the abundance of several metabolites used in the hexosamine biosynthesis pathway (HBP) for the synthesis of UDP-GlcNAc were higher, including glutamine, glucose and acetyl-CoA (Figure 3B). These findings suggest that Th2-DCs specifically upregulate HBP flux to fuel O-GlcNAcylation. To better determine if this metabolic module is unique to Th2-DCs, we compared the mRNA expression of enzymes in the HBP and O-GlcNAcylation pathway between Th2- and Th1- and Th17-DCs. OGT mRNA was specifically upregulated in Th2-DCs compared to differently conditioned DCs, although this did not appear to translate into higher OGT protein expression 24 hours after stimulation with omega-1 (Figure S4B). In contrast, MGEA5 mRNA was upregulated in all Th-polarizing DCs compared to iDCs. Th2-DCs displayed higher expression of NAGK (also known as GNK) than Th1-DCs and Th17-DCs, while conversely, Th1-DCs and Th17-DCs showed higher expression of the rate-limiting enzymes of the HBP, GFPT1 and GFPT2 (also known as GFAT; Figure 3C). These data may suggest that Th2-DCs utilize different fuels for hexosamine synthesis than Th17- or Th1-DCs, as NAGK, the enzyme that mediates the conversion of glucosamine into glucosamine-6-phosphate, bypasses the need for glucose and glutamine by using glucosamine.

Taken together, these data show that in addition to suppressed glycolysis, Th2-priming DC are metabolically wired to increase synthesis of UDP-GlcNAc and other hexosamines, which may be used for supporting protein O-GlcNAcylation.

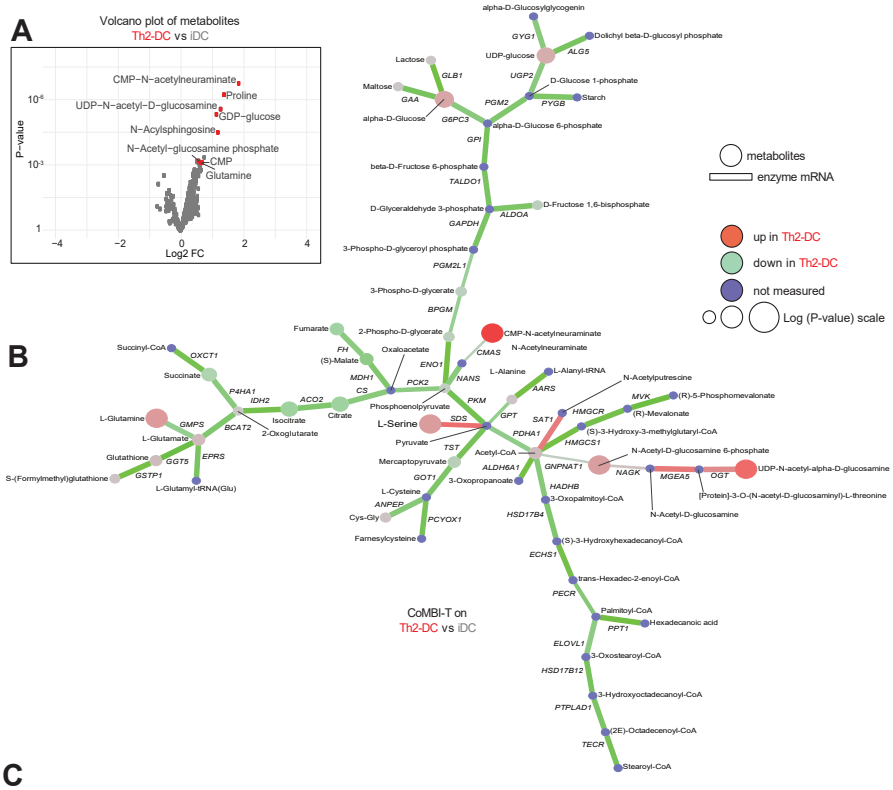
A
Volcano plot of metabolites
Th2-DC vs iDC
CMP−N−acetylneuraminate
Proline
UDP−N−acetyl−D−glucosamine
GDP−glucose
N−Acylsphingosine
N−Acetyl−glucosamine phosphate
CMP
Glutamine
P−value
Log2 FC
B
CoMBI-T on
Th2-DC vs iDC
metabolites
enzyme mRNA
up in Th2-DC
down in Th2-DC
not measured
Log (P-value) scale
C
GFPT1 mRNA (log2 relative)
GFPT2
NAGK
GNPNAT
PGM3 mRNA (log2 relative)
UAP1
OGT
MGEA5
iDC
Th1-DC
Th17-DC
Th2-DC

Figure 3. Integration of transcriptomic and metabolomic data reveals that enhanced hexosamine biosynthesis and O-GlcNAc transferase expression are unique to Th2-priming DCs.

Human moDCs were left untreated (iDC in grey) or stimulated for 24h with either LPS+PolyIC (Th1-DC in dark blue), zymosan (Th17-DC in green) or omega-1 (Th2-DC in red). DCs were then set aside for either flow injection analysis mass spectrometry (FIA-MS; A) or RNA-sequencing (C). Metabolomic and transcriptomic data sets were furthermore integrated using the GAM tool (B).
(A) Volcano plot showing metabolites differentially expressed between Th2-DC and iDC conditions. X axis shows log-fold change between Th2-DC and iDC conditions with positive values corresponding to metabolites upregulated in Th2-DCs. Y axis shows p value for corresponding metabolite. Top Th2-DC-specific metabolites are highlighted in red.
(B) Most regulated subnetwork within the global human metabolic network that consists of enzymes and metabolites through the CoMBI-T profiling pipeline. Round nodes represent metabolites within core regulatory network. Enzymes are represented by square nodes. Differential expression of corresponding enzyme/metabolite is indicated by the size of the node, and fold-change by red (Th2-DC) to green (iDC) color scale. Enzymes in reactions with single product-substrate pair are represented by edges for visual convenience with thickness and color of the edge reflecting -log(p) and fold-change of differential expression correspondingly.
(C) Relative log mRNA expression of enzymes involved in protein O-GlcNAcylation (OGT and MGEA5) and the hexosamine biosynthesis pathway (HBP; rest) between differently conditioned DCs.

O-GlcNAcylation is required for Th2 priming by DCs but not for Th1 or Th17 priming

We next aimed to investigate if this signature of HBP activity and OGT expression was of functional importance to Th2-DCs. Inhibition of OGT using the pharmacological inhibitor ST045849 abolished the capacity of Th2-DCs to prime IL-4-producing Th2 cells, while the proportion of IFNγ-producing Th1 cells was not affected in these conditions (Figure 4A-B). Knockdown of OGT – using short interfering RNA – also abolished the Th2-priming capacity of Th2-DCs as well as their ability to suppress Th1 responses (Figure 4C). These T cells did not start producing IL-17 (Figure S5A) nor was their viability affected (Figure S5A-C). Importantly, OGT blockade in Th1- and Th17-DCs did not compromise their Th cell-polarizing ability (Figure 4D-E). This suggests a unique role for OGT-driven O-GlcNAcylation in the conditioning of DCs for Th2 priming. Interestingly, global protein O-GlcNAcylation levels as determined by flow cytometry (Figure 4F) and immunoblotting (Figure 4G) were similar between Th2-DCs and iDCs. This shows that the increased UDP-GlcNAc availability does not translate into an overall increased protein O-GlcNAcylation in Th2-DCs, but instead suggests that O-GlcNAcylation of a select number of proteins is potentially of importance for Th2 priming by DCs. UDP-GlcNAc can also serve as a substrate for N- and O-glycosylation. However, the N-glycosylation inhibitor tunicamycin did not affect the Th2-priming capacity of Th2-DCs (Figure 4A-B). Instead it specifically

limited the ability of Th1-DCs to induce IFNγ production by T cells (Figure 4E) without promoting a switch to a different Th phenotype (Figure S5D-E). Neither ST045849 treatment, nor OGT silencing or tunicamycin treatment negatively impacted DC survival (Figure S5-F-G). Taken together, these data show that the transfer of GlcNAc from UDP-GlcNAc onto proteins by OGT is uniquely important for Th2 priming by DCs.

To start exploring mechanistically how O-GlcNAcylation in DCs is linked to their Th2-priming capacity, we first assessed whether silencing of OGT prevented surface marker expression or cytokine secretion by Th2-DCs. However, silencing of OGT did not change MHCII and CD40 surface expression (Figure S6A) nor IL-12 and IL-10 secretion (Figure S6A). Recent reports have implicated type I IFN signaling in DC-driven Th2 responses *in vivo* [24, 26]. Moreover, it was recently demonstrated that O-GlcNAcylation of mitochondrial anti-viral-signaling protein (MAVS) can enhance the interferon regulatory factor 3 (IRF3)-mediated production of type I IFNs [27]. Indeed, a non-targeted approach by performing gene set enrichment analysis on the differentially expressed genes between Th2-DCs and iDCs revealed type I interferon (IFN) signaling as the top pathway differentiating Th2-DCs from iDCs (Figure S6C). This may provide a first lead through which mechanism O-GlcNAcylation supports Th2 priming by DCs.

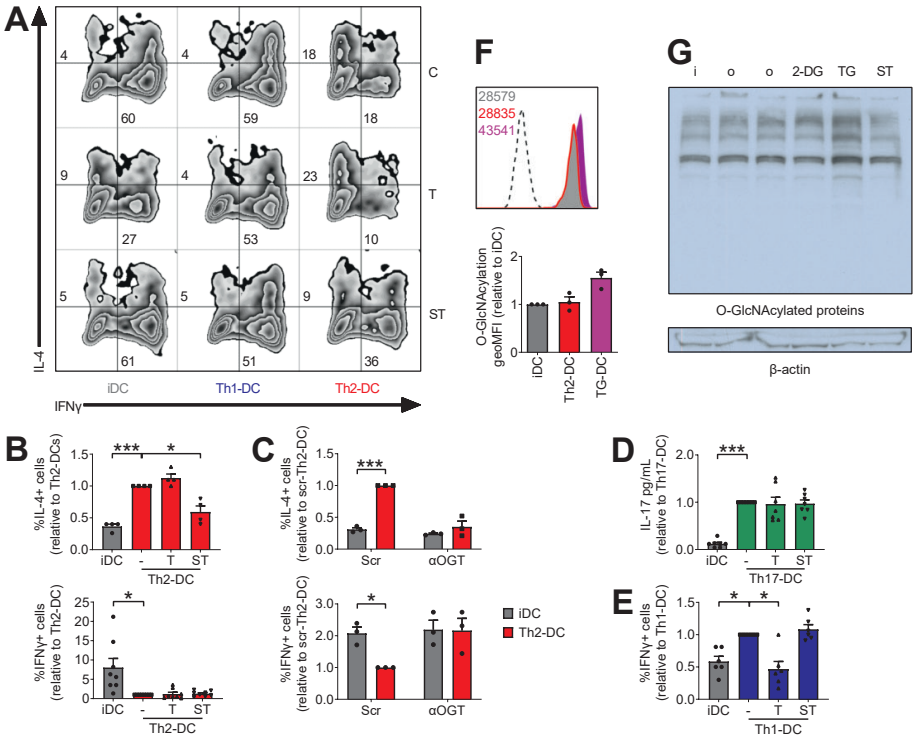

Figure 4. O-GlcNAcylation is required for Th2 priming by DCs but not for Th1 or Th17 priming.

Human moDCs were differentiated as normally (A-B, D-G) or short interfering RNA was introduced against O-GlcNAc transferase (OGT) at day 4 (C). Scrambled RNA was used as a control. At day 6, DCs were stimulated as normal with either LPS+PolyIC (Th1-DC in dark blue), zymosan (Th17-DC in green), omega-1 (Th2-DC in red / o), 2-deoxyglucose (2-DG-DC in white / 2-DG), Thiamet G (TG-DC in black / TG) or ST045849 (ST) for 24 hours, left untreated (iDC in grey / i), or first pre-incubated with inhibitors of O-GlcNAcylation (ST045849 [ST]), N-glycosylation (tunicamycin [T] for 30 minutes, or left untreated [C]. DCs were then set aside for either co-culture with allogeneic T cells (A-E) or determination of overall protein O-GlcNAcylation using flow cytometry (F) or western blotting (G).
(A) Representative histograms of T cell intracellular IFNγ and IL-4 that was analyzed by flow cytometry after a 6h stimulation with phorbol myristate acetate (PMA) and ionomycin. T cells used were naïve and the culture was 11 days.
(B-C, E) Co-culture with naïve T cells for 11 days. The percentages of T cells uniquely positive for either IFNγ or IL-4 are expressed relatively.
(D) Co-culture with memory T cells. Supernatants were collected after 5 days and IL-17 concentrations was determined by ELISA.
(F) Flow cytometry-based analysis of overall protein O-GlcNAcylation. Dotted line represents the fluorescence minus one control and Thiamet G – an inhibitor of O-GlcNAcase - was used a positive control.
(G) Western blot-based analysis of overall protein O-GlcNAcylation. Thiamet G was used a positive control and ST045849 - an inhibitor of O-GlcNAc transferase – was used as

a negative control. Beta-actin was taken along as housekeeping protein.

Allergen and 2-DG-driven Th2 priming by DCs depends on O-GlcNAcylation

To determine whether this metabolic profile of omega-1-conditioned DCs is a feature of Th2-priming DCs in general, we additionally assessed whether house dust mite allergen extract-conditioned DCs (HDM-DCs) would share the glycolytic and OGT sensitive profile of Th2-DCs conditioned with omega-1. On both accounts the HDM-DCs phenocopied omega-1-conditioned Th2-DCs, as conditioning with HDM also diminished the rapid induction of glycolysis by LPS (Figure 5A) and the Th2 priming-capacity of HDM-DCs was abolished by ST045849 (Figure 5B). Likewise, Th2 induction by 2-DG-DCs was impaired by OGT inhibition (Figure 5C), suggesting not only that O-GlcNAcylation in DCs is a general requirement for Th2-polarization, but also that reduction in glycolysis and O-GlcNAcylation are functionally linked.

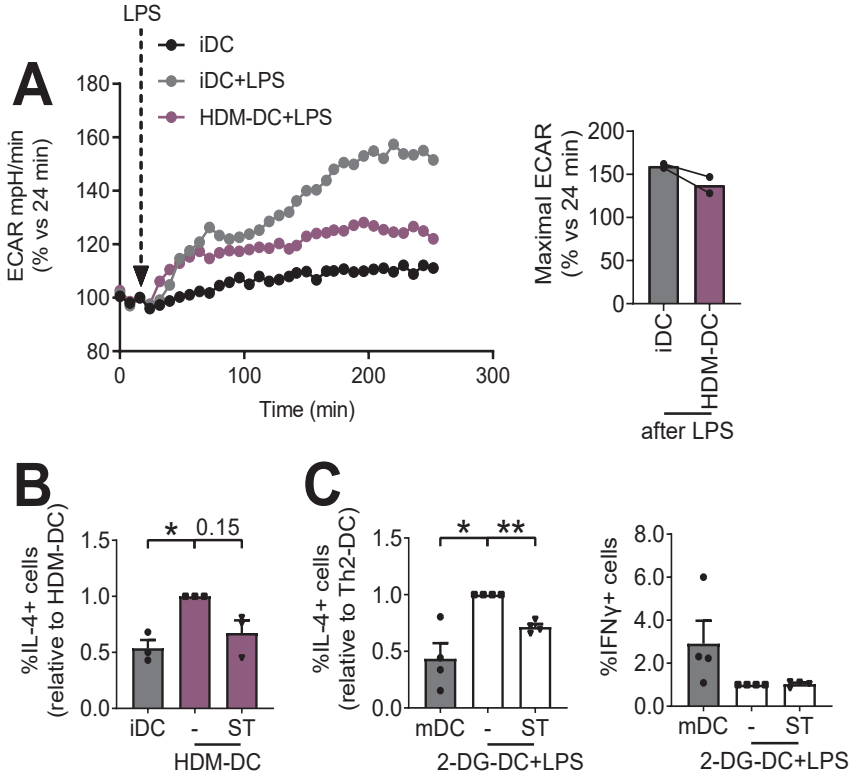

Figure 5. Allergen-induced Th2 priming by DCs also requires O-GlcNAcylation.

Human moDCs were left untreated (iDC in grey) or stimulated for 24h with house dust mite (HDM-DC in purple). DCs were then set aside for measurements of glycolysis using

extracellular flux (XF) analysis (A) or co-culture with allogeneic T cells (B).
(A) Co-culture with naïve T cells for 11 days. T cell intracellular IFNγ and IL-4 was analyzed by flow cytometry after a 6h stimulation with phorbol myristate acetate (PMA) and ionomycin. The percentages of T cells uniquely positive for IL-4 are expressed relatively.
(B) Real-time changes in the ECAR of DCs treated with LPS.
(C) Day 6 moDCs were stimulated either with LPS only (mDC in grey) or 2-deoxyglucose (2-DG-DC in white) in the presence of LPS. Some cells were first pre-incubated with an inhibitor of O-GlcNAcylation (ST045849 [ST]) for 30 minutes. The next day, DCs were set aside for co-culture with allogeneic T cells as in Figure 5A.

cDC2s from helminth infection individuals are characterized by increased protein O-GlcNAcylation

Finally, to study the *in vivo* relevance of our findings, we examined whether protein O-GlcNAcylation was affected in peripheral blood DCs of participants taking part in a controlled human infection (CHI) study using *Necator americanus* [28]. Eight weeks post infection, around the peak of the type 2 immune response as determined by eosinophilia (Figure 6A), protein O-GlcNAcylation was detected by flow cytometry. O-GlcNAcylation was increased in type 2 conventional DCs (cDC2s) - the subset that is classically associated with the priming of Th cell responses [29] - but not plasmacytoid DCs or cDC1s (Figure 6B). This increase shows that enhanced protein O-GlcNAcylation is also a characteristic of DCs during an active type 2 immune response in humans.

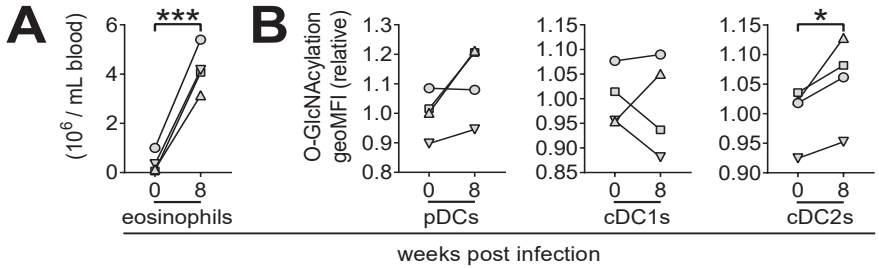

Figure 6. cDC2s from helminth infection individuals are characterized by increased O-GlcNAcylation.

Volunteers were infected with the hookworm *Nector americanus* for 8 weeks in a controlled human infection study. Induction of type 2 immune responses was determined by quantification of eosinophilia in blood using flow cytometry (A). Global protein O-GlcNAcylation in peripheral blood CD123+ plasmacytoid DCs (pDCs), CD141+ type 1 conventional DCs (cDC1s) and CD1c+ cDC2s was assessed using flow cytometry (B).

Discussion

Given the paucity in our understanding of the role of cellular metabolism in Th2 polarization by DCs, we aimed in the present study to identify metabolic properties that are unique to DCs that induce Th2 polarization and to determine the functional importance of those metabolic programs in DCs in priming this response. We found that Th2-priming DCs can be distinguished from immature iDCs, Th1- and Th17-priming DCs based on low glycolytic activity, a characteristic being in itself sufficient to endow DCs with Th2-polarizing ability. Another metabolic module that was found to not only define Th2-priming DCs, but also to be required for their ability to drive Th2 polarization, was the HBP and the associated process of O-GlcNAcylation. Importantly, we provide evidence that this relation between glycolysis, O-GlcNAcylation and Th2 priming extends beyond helminth antigen-conditioned *in vitro* Th2-DCs, as stimulation with allergenic HDM also impaired glycolytic flux and in addition promoted OGT-sensitive Th2 priming. Moreover, type 2 cDCs in peripheral blood from hookworm-infected individuals showed increased overall protein O-GlcNAcylation, while cDC1s and pDCs did not.

As opposed to DCs that prime Th1 or Th17 responses, Th2-priming DCs are commonly characterized by a muted activation phenotype and low expression of pro-inflammatory cytokines, of which particularly low IL-12 expression and low antigen presentation have been linked to their ability to prime Th2 responses [30]. Induction of aerobic glycolysis has been shown to be associated with and required for acquisition immunogenic DC activation and production of Th1-polarizing signals such as IL-12 [7, 8, 10]. Mechanistically, this has been linked to glycolysis-driven fatty acid synthesis that allows for ER/Golgi expansion in DCs after TLR ligation [8], which is thought necessary for optimal expression of costimulatory molecules and T cell-polarizing cytokines. Therefore, the impaired glycolytic potential of Th2-DCs we observed on our work may 'lock' them into a muted activation phenotype to allow for efficient Th2 priming. Indeed, inhibition of glycolysis itself made DCs refractory to secrete IL-12 following CD40 ligation and was sufficient to condition DCs for Th2 priming.

How omega-1 would suppress glycolysis is still unclear. It is a protein that bears N-glycans with terminal Lewis-X [fucosylated Galβ1-4(Fucα1-3)GlcNAc] motifs and has T2 ribonuclease (RNase) activity [17, 31]. Both protein glycosylation and RNase activity are required to drive Th2 responses [17]. One possibility is that omega-1 through its RNase activity and ability to suppress global protein synthesis also compromises the expression of glycolytic enzymes. In addition, it was recently reported that the triggering of galactose-type lectin receptor (MGL), which recognizes N-acetylgalactosamine (GalNAc) residues [32], reduces

glycolysis in moDCs [33]. Although omega-1 recognition and internalization by DCs has been reported to be primarily mediated via the mannose receptor [17], it is conceivable it may also bind to macrophage galactose-type lectin receptor (MGL) through its terminal GalNAc residues that are present at a low frequency on its glycans [34]. Therefore, this omega-1-MGL interaction may additionally contribute to suppression of glycolysis in omega-1-conditioned moDCs.

The muted activation phenotype, underpinned by impaired glycolytic reprogramming, would be largely consistent with the 'default concept' [22, 35], which postulates that the absence of Th1-polarizing signals leads - by default - to a Th2 outcome [3]. However, this default concept has been challenged by studies showing a role for ligands of the Notch receptor (Jagged 1 and 2) and the TNF receptor superfamily (OX40L) in Th2 polarization by DCs in certain context [36-40], although blockade of these pathways did not prevent Th2 priming *in vivo* [41, 42]. Therefore, immunological signals that can uniformly distinguish Th2-priming DCs from other DCs are still unknown [4]. Here, we identified a positive metabolic signature that is unique for Th2-DCs defined by elevated levels of HBP metabolites and OGT mRNA. Although we did not find increased total O-GlcNAcylation in Th2-DCs after 24 hours of conditioning, the fact that Th2-DCs were singularly sensitive to OGT inhibition – both pharmacologically and genetically – indicates that some proteins need to be O-GlcNAcylated for a proper activation of a Th2-priming program in these DCs to ensue.

A key question is how O-GlcNAcylation underpins the ability of DCs to prime Th2 responses. The investigation of how O-GlcNAcylation - as a post-translational modification of proteins - effects the function of immune cells is still in its infancy, but is gaining traction [43]. The role of O-GlcNAcylation has been more exhaustively studied in cancer where it has an important function in the glycolytic reprogramming of cancer cells [44]. Key enzymes in glycolysis such as hexokinase (HK), phosphofructokinase (PFK) and pyruvate kinase isozyme M2 (PKM2) can all be O-GlcNAcylated, resulting in change in glycolytic flux [45]. Whether a similar functional connection between O-GlcNAcylation and inhibition in glycolysis exists in human DCs remains to be determined. However, since pharmacological inhibition of OGT did not rescue omega-1-mediated suppression of IL-12 production, which we show is a consequence of low glycolytic rates, this seems unlikely.

Possibly a more plausible explanation for how O-GlcNAcylation may regulate Th2 priming by DCs, comes from our transcriptomic analysis identifying type I IFN signaling as the top pathway that could distinguish Th2-DCs from iDCs. Recent studies have reported that type I IFN signaling in cDCs is required for Th2 induction *in vivo* in several murine models of type 2 immunity [24, 26] and

MAVS - as a central adaptor molecule required for production of type I IFNs - depends on O-GlcNAcylation for its activity [27, 46, 47]. Therefore, a role for O-GlcNAcylation in conditioning DCs for Th2 priming through control of type 1 IFN signaling is conceivable. Further work is needed to determine a possible relation between O-GlcNAcylation, type I IFN-related cytokine production and Th2 priming by DCs.

Another observation was that Th2 priming following pharmacological inhibition of glycolysis in DCs was largely dependent on O-GlcNAcylation. In T cells, it has been shown that high rates of anaerobic glycolysis limits flux of glucose-derived metabolites into the HBP and thereby UDP-GlcNAc synthesis. Conversely, suppression of glycolysis allows for redirection of glucose into the HBP resulting in enhanced UDP-GlcNAc [48]. Also in liver, neuronal and lung cancer cell lines, this inverse relation has been reported with increases in OGT expression and protein O-GlcNAcylation after glucose deprivation [49-52]. This makes it conceivable that in Th2-DCs, active suppression of glycolysis may not only be a prerequisite for Th2 induction by limiting their IL-12 expression and restricting overall maturation, but also for increased HBP flux, UDP-GlcNAc synthesis and O-GlcNAcylation. This subsequently provides a yet to be identified additional signal(s) that license(s) DCs to prime a Th2 response as discussed above.

Finally, we extend our *in vitro* observations to primary DCs in humans, by showing that cDC2s from individuals taking part in a controlled human hookworm infection trial, displayed increased intracellular O-GlcNAcylation levels during the peak of their type 2 immune response. The finding that this change in O-GlcNAcylation was only consistently observed in CD1c+ cDC2s, but not cDC1s or pDCs, and the knowledge that particularly this DC subset has been linked to regulation of Th cell responses in humans [53-55], provides a first indication that O-GlcNAcylation is also important for DCs to drive Th2 responses in the context of human helminth infection. Further studies are warranted to test this hypothesis and assess the functional relevance of this increased O-GlcNAcylation signature in Th cell polarization by cDC2s.

In summary, we identified HBP, O-GlcNAcylation and low glycolysis as key metabolic processes that uniquely define Th2-priming DCs and that underpin their ability to prime this response. How these different processes exactly interact is not yet clear. More research is needed to elucidate this interplay and how Th2-priming DCs maintain essential HBP flux in the context of suppressed glycolysis. However, their unique characteristics of high HBP engagement and protein O-GlcNAcylation can provide an opportunity for DC manipulation of

their Th2-priming capacity through targeting these pathways without affecting Th1- or Th17-priming.

References

1. Gause, W.C., C. Rothlin, and P. Loke, *Heterogeneity in the initiation, development and function of type 2 immunity.* Nat Rev Immunol, 2020. **20**(10): p. 603-614.
2. Kapsenberg, M.L., *Dendritic-cell control of pathogen-driven T-cell polarization.* Nat Rev Immunol, 2003. **3**(12): p. 984-93.
3. MacDonald, A.S. and R.M. Maizels, *Alarming dendritic cells for Th2 induction.* J Exp Med, 2008. **205**(1): p. 13-7.
4. Schuijs, M.J., H. Hammad, and B.N. Lambrecht, *Professional and 'Amateur' Antigen-Presenting Cells In Type 2 Immunity.* Trends Immunol, 2019. **40**(1): p. 22-34.
5. O'Neill, L.A. and E.J. Pearce, *Immunometabolism governs dendritic cell and macrophage function.* J Exp Med, 2016. **213**(1): p. 15-23.
6. Pearce, E.J. and B. Everts, *Dendritic cell metabolism.* Nat Rev Immunol, 2015. **15**(1): p. 18-29.
7. Patente, T.A., L.R. Pelgrom, and B. Everts, *Dendritic cells are what they eat: how their metabolism shapes T helper cell polarization.* Curr Opin Immunol, 2019. **58**: p. 16-23.
8. Everts, B., et al., *TLR-driven early glycolytic reprogramming via the kinases TBK1-IKKvarepsilon supports the anabolic demands of dendritic cell activation.* Nat Immunol, 2014. **15**(4): p. 323-32.
9. Guak, H., et al., *Glycolytic metabolism is essential for CCR7 oligomerization and dendritic cell migration.* Nat Commun, 2018. **9**(1): p. 2463.
10. Krawczyk, C.M., et al., *Toll-like receptor-induced changes in glycolytic metabolism regulate dendritic cell activation.* Blood, 2010. **115**(23): p. 4742-9.
11. Thwe, P.M., et al., *Cell-Intrinsic Glycogen Metabolism Supports Early Glycolytic Reprogramming Required for Dendritic Cell Immune Responses.* Cell Metab, 2017. **26**(3): p. 558-567.e5.
12. Fliesser, M., et al., *Hypoxia-inducible factor 1alpha modulates metabolic activity and cytokine release in anti-Aspergillus fumigatus immune responses initiated by human dendritic cells.* Int J Med Microbiol, 2015. **305**(8): p. 865-73.
13. Ferreira, G.B., et al., *Vitamin D3 Induces Tolerance in Human Dendritic Cells by Activation of Intracellular Metabolic Pathways.* Cell Rep, 2015. **10**(5): p. 711-725.
14. Malinarich, F., et al., *High mitochondrial respiration and glycolytic capacity represent a metabolic phenotype of human tolerogenic dendritic cells.* J Immunol, 2015. **194**(11): p. 5174-86.
15. Zhao, F., et al., *Paracrine Wnt5a-beta-Catenin Signaling Triggers a Metabolic Program that Drives Dendritic Cell Tolerization.* Immunity, 2018. **48**(1): p. 147-160.e7.
16. Jha, A.K., et al., *Network integration of parallel metabolic and transcriptional data reveals metabolic modules that regulate macrophage polarization.* Immunity, 2015. **42**(3): p. 419-30.
17. Everts, B., et al., *Schistosome-derived omega-1 drives Th2 polarization by suppressing protein synthesis following internalization by the mannose receptor.* J Exp Med, 2012. **209**(10): p. 1753-67, s1.
18. Everts, B., et al., *Omega-1, a glycoprotein secreted by Schistosoma mansoni eggs, drives Th2 responses.* J Exp Med, 2009. **206**(8): p. 1673-80.

19. Steinfelder, S., et al., *The major component in schistosome eggs responsible for conditioning dendritic cells for Th2 polarization is a T2 ribonuclease (omega-1).* J Exp Med, 2009. **206**(8): p. 1681-90.
20. Hilligan, K.L., et al., *Dermal IRF4+ dendritic cells and monocytes license CD4+ T helper cells to distinct cytokine profiles.* Nat Commun, 2020. **11**(1): p. 5637.
21. Hussaarts, L., et al., *Rapamycin and omega-1: mTOR-dependent and -independent Th2 skewing by human dendritic cells.* Immunol Cell Biol, 2013. **91**(7): p. 486-9.
22. Hussaarts, L., M. Yazdanbakhsh, and B. Guigas, *Priming dendritic cells for th2 polarization: lessons learned from helminths and implications for metabolic disorders.* Front Immunol, 2014. **5**: p. 499.
23. Janss, T., et al., *Interferon response factor-3 promotes the pro-Th2 activity of mouse lung CD11b(+) conventional dendritic cells in response to house dust mite allergens.* Eur J Immunol, 2016. **46**(11): p. 2614-2628.
24. Webb, L.M., et al., *Type I interferon is required for T helper (Th) 2 induction by dendritic cells.* Embo j, 2017. **36**(16): p. 2404-2418.
25. Sergushichev, A.A., et al., *GAM: a web-service for integrated transcriptional and metabolic network analysis.* Nucleic Acids Res, 2016. **44**(W1): p. W194-200.
26. Connor, L.M., et al., *Th2 responses are primed by skin dendritic cells with distinct transcriptional profiles.* J Exp Med, 2017. **214**(1): p. 125-142.
27. Song, N., et al., *MAVS O-GlcNAcylation Is Essential for Host Antiviral Immunity against Lethal RNA Viruses.* Cell Rep, 2019. **28**(9): p. 2386-2396.e5.
28. Hoogerwerf, M.A., et al., *New Insights Into the Kinetics and Variability of Egg Excretion in Controlled Human Hookworm Infections.* J Infect Dis, 2019. **220**(6): p. 1044-1048.
29. Eisenbarth, S.C., *Dendritic cell subsets in T cell programming: location dictates function.* Nat Rev Immunol, 2019. **19**(2): p. 89-103.
30. van Panhuys, N., F. Klauschen, and R.N. Germain, *T-cell-receptor-dependent signal intensity dominantly controls CD4(+) T cell polarization In Vivo.* Immunity, 2014. **41**(1): p. 63-74.
31. Dunne, D.W., F.M. Jones, and M.J. Doenhoff, *The purification, characterization, serological activity and hepatotoxic properties of two cationic glycoproteins (alpha 1 and omega 1) from Schistosoma mansoni eggs.* Parasitology, 1991. **103 Pt 2**: p. 225-36.
32. Meevissen, M.H., et al., *Specific glycan elements determine differential binding of individual egg glycoproteins of the human parasite Schistosoma mansoni by host C-type lectin receptors.* Int J Parasitol, 2012. **42**(3): p. 269-77.
33. Zaal, A., et al., *Activation of the C-Type Lectin MGL by Terminal GalNAc Ligands Reduces the Glycolytic Activity of Human Dendritic Cells.* Front Immunol, 2020. **11**: p. 305.
34. Meevissen, M.H., et al., *Structural characterization of glycans on omega-1, a major Schistosoma mansoni egg glycoprotein that drives Th2 responses.* J Proteome Res, 2010. **9**(5): p. 2630-42.
35. Jankovic, D., et al., *In the absence of IL-12, CD4(+) T cell responses to intracellular pathogens fail to default to a Th2 pattern and are host protective in an IL-10(-/-) setting.* Immunity, 2002. **16**(3): p. 429-39.

36. Amsen, D., et al., *Instruction of distinct CD4 T helper cell fates by different notch ligands on antigen-presenting cells.* Cell, 2004. **117**(4): p. 515-26.
37. Balic, A., et al., *Selective maturation of dendritic cells by Nippostrongylus brasiliensis-secreted proteins drives Th2 immune responses.* Eur J Immunol, 2004. **34**(11): p. 3047-59.
38. de Kleer, I.M., et al., *Perinatal Activation of the Interleukin-33 Pathway Promotes Type 2 Immunity in the Developing Lung.* Immunity, 2016. **45**(6): p. 1285-1298.
39. Ito, T., et al., *TSLP-activated dendritic cells induce an inflammatory T helper type 2 cell response through OX40 ligand.* J Exp Med, 2005. **202**(9): p. 1213-23.
40. Willart, M.A., et al., *Interleukin-1α controls allergic sensitization to inhaled house dust mite via the epithelial release of GM-CSF and IL-33.* J Exp Med, 2012. **209**(8): p. 1505-17.
41. Chu, D.K., et al., *IL-33, but not thymic stromal lymphopoietin or IL-25, is central to mite and peanut allergic sensitization.* J Allergy Clin Immunol, 2013. **131**(1): p. 187-200.e1-8.
42. Tu, L., et al., *Notch signaling is an important regulator of type 2 immunity.* J Exp Med, 2005. **202**(8): p. 1037-42.
43. Quik, M., C.H. Hokke, and B. Everts, *The role of O-GlcNAcylation in immunity against infections.* Immunology, 2020. **161**(3): p. 175-185.
44. Jozwiak, P., et al., *O-GlcNAcylation and Metabolic Reprograming in Cancer.* Front Endocrinol (Lausanne), 2014. **5**: p. 145.
45. Yi, W., et al., *Phosphofructokinase 1 glycosylation regulates cell growth and metabolism.* Science, 2012. **337**(6097): p. 975-80.
46. Li, T., et al., *O-GlcNAc Transferase Links Glucose Metabolism to MAVS-Mediated Antiviral Innate Immunity.* Cell Host Microbe, 2018. **24**(6): p. 791-803.e6.
47. Seo, J., et al., *O-Linked N-Acetylglucosamine Modification of Mitochondrial Antiviral Signaling Protein Regulates Antiviral Signaling by Modulating Its Activity.* Front Immunol, 2020. **11**: p. 589259.
48. Araujo, L., et al., *Glycolysis and glutaminolysis cooperatively control T cell function by limiting metabolite supply to N-glycosylation.* Elife, 2017. **6**.
49. Cheung, W.D. and G.W. Hart, *AMP-activated protein kinase and p38 MAPK activate O-GlcNAcylation of neuronal proteins during glucose deprivation.* J Biol Chem, 2008. **283**(19): p. 13009-20.
50. Kang, J.G., et al., *O-GlcNAc protein modification in cancer cells increases in response to glucose deprivation through glycogen degradation.* J Biol Chem, 2009. **284**(50): p. 34777-84.
51. Taylor, R.P., et al., *Up-regulation of O-GlcNAc transferase with glucose deprivation in HepG2 cells is mediated by decreased hexosamine pathway flux.* J Biol Chem, 2009. **284**(6): p. 3425-32.
52. Taylor, R.P., et al., *Glucose deprivation stimulates O-GlcNAc modification of proteins through up-regulation of O-linked N-acetylglucosaminyltransferase.* J Biol Chem, 2008. **283**(10): p. 6050-7.
53. Bachem, A., et al., *Superior antigen cross-presentation and XCR1 expression define human CD11c+CD141+ cells as homologues of mouse CD8+ dendritic cells.* J Exp Med, 2010. **207**(6): p. 1273-81.

54. Leal Rojas, I.M., et al., *Human Blood CD1c(+) Dendritic Cells Promote Th1 and Th17 Effector Function in Memory CD4(+) T Cells.* Front Immunol, 2017. **8**: p. 971.
55. Yin, X., et al., *Human Blood CD1c+ Dendritic Cells Encompass CD5high and CD5low Subsets That Differ Significantly in Phenotype, Gene Expression, and Functions.* J Immunol, 2017. **198**(4): p. 1553-1564.
56. Vincent, E.E., et al., *Mitochondrial Phosphoenolpyruvate Carboxykinase Regulates Metabolic Adaptation and Enables Glucose-Independent Tumor Growth.* Mol Cell, 2015. **60**(2): p. 195-207.
57. Gainullina, A., et al., *Open Source ImmGen: network perspective on metabolic diversity among mononuclear phagocytes.* bioRxiv, 2020.
58. Ulland, T.K., et al., *TREM2 Maintains Microglial Metabolic Fitness in Alzheimer's Disease.* Cell, 2017. **170**(4): p. 649-663.e13.
59. Pelgrom, L.R., A.J. van der Ham, and B. Everts, *Analysis of TLR-Induced Metabolic Changes in Dendritic Cells Using the Seahorse XF(e)96 Extracellular Flux Analyzer.* Methods Mol Biol, 2016. **1390**: p. 273-85.

Methods

Isolation of peripheral blood mononuclear cells

Peripheral venous blood, from buffy coats provided by Sanquin (Amsterdam, The Netherlands), was divided in conical 50 mL tubes (#227261, Greiner) with 20 mL of room temperature venous blood diluted 1:1 with room temperature HBSS (#14170-088, Gibco) per tube. This solution was gently mixed before addition of 13 mL room temperature Ficoll (#17-1440-02, GE healthcare) underneath the blood:HBSS. Alternatively, all liquids were used cold, but temperatures were never mixed. Peripheral blood mononuclear cells (PBMCs) were concentrated into a ring by density centrifugation at 400g with low brake for 25 minutes at room temperature. The rings were transferred using a Pasteur pipette (#861172001, Sarstedt) to new 50 mL tubes to which HBSS supplemented with 1% v/v heat-inactivated fetal calf serum (HI-FCS; #S-FBS-EU-015, Serana, Pessin, Germany) was added up to 50 mL. Blood platelets were removed by two rounds of centrifugation at 200g with normal brake for 20 minutes at room temperature. Finally, the PBMCs were resuspended in a home-made cell separation buffer (MACS buffer = PBS [from LUMC pharmacy] supplemented with 0.5% BSA [fraction V, #10735086001, Roche, Woerden, The Netherlands] and 2 mM EDTA [#15575-038, Thermo]) that was sterilized using a 0.22 µm filter system (#431097, Corning).

Monocyte-derived dendritic cell culture

PBMCs were counted using an in-house Türk solution (= 50 mg gentian violet, 5 mL glacial acetic acid and 500 mL H_20) and brought to a concentration of 10^7 cells per 95 µL of MACS buffer. Monocytes were isolated by addition of 5 µL of CD14 MACS beads (#120-007-943, Miltenyi) per 10^7 cells, mixing well, incubating for 15 minutes at 4 degrees Celsius and column sorting using LS columns (#130-042-401, Miltenyi) according to the manufacturer's protocol provided with the beads. Whole PBMCs, CD14- flow through and CD14+ monocyte fractions were set aside to check for purity, which routinely was >95%. Monocytes were brought to 400 cells per µL in ice-cold monocyte-derived dendritic cell (moDC) differentiation medium (= no additives RPMI [naRPMI; #42401-042, Invitrogen] supplemented with 10% HI-FCS, 2 mM L-glutamine [#G-8540-100g, Sigma], 100 U/mL penicillin [#16128286, Eureco-pharma , Ridderkerk, The Netherlands] and 100 µg/mL streptomycin [#S9137, Sigma] that together formed our general human immune cell RPMI for metabolism work or 'himRPMI' and also 10 ng/mL of human recombinant granulocyte/ macrophage colony-stimulating factor (GM-CSF; #PHC2013, Biosource) and 0.86 ng/mL of human recombinant IL-4 (#204-IL, R&D systems) was added for moDC differentiation. The media was kept cold to prevent monocytes sticking to the plastic tube. Monocytes were usually plated at 2 million cells per 5 mL

of media in 6-well plates (#140675, Nunc) and after 2 or 3 days, the top half of the medium was carefully removed and replaced by 2.5 mL of fresh medium complemented with 20 ng/mL of GM-CSF and 1.72 ng/mL of IL-4 to maintain the concentrations of differentiating cytokines.

O-GlcNAc transferase knockdown

At day 4 of the culture, the cells were harvested, washed with PBS, brought to a concentration of 1.1x10^6 cells per 100 µL and split into 1.5 mL Eppendorf tubes with 100 µL of cell solution. Shortly before transfection by electroporation, tubes were spun down, cell pellets were carefully pipetted dry, pellets were reconstituted in 100 µL of resuspension buffer and 10 µL of 455 nM siRNA was added (anti-OGT [#M-019111-00-0005, Darmacon, Lafayette, Colorado, United States] or scrambled control [#D-001206-13-05, Darmacon]). Electroporation as described here was performed using the 100 µL variant (#MPK10096, Invitrogen) of the Neon Transfection System (#MPK5000, Invitrogen) and a complementary pipette (#MPP100, Invitrogen) with the following settings: 1600 V, 20 ms and one pulse. Immediately after electroporation, the cells were transferred to 5 mL of 10% HI-FCS RPMI-1640 with 2 mM glutamine but without further additions. Importantly, the media contained no antibiotics at this stage. Electroporation tips were re-used to a maximum of three times for the same target. Later, the cells were plated at 200 cells per µL in, if cell numbers allowed it, 6-well plates again. The next morning, the media was re-supplemented with penicillin, streptomycin, rGM-CSF and rIL-4. At day 6, the cells were handled as normally. Reconstituting the pellet in a total volume of 110 µL helped prevent sucking up air bubbles into the electroporation tip, which is crucial. Minimizing time spend in the resuspension buffer helped with cell viability. Silencing efficiency was determined by qPCR on 6 days old cells and was routinely greater than 80%.

DC stimulation and analysis of activation

Day 5-7 moDCs were harvested without discarding the differentiation media and replated in 96-well plates (#167008, Nunc) at 5-10x10^4 cells per 100 µL of the same media and left to rest for 2-3 hours. Alternatively, cells were plated in 200 µL and the next day the top half of the medium was carefully removed. Inhibitors were added 30 minutes prior to antigen stimulation and the cells were kept for a total of 24 hours in a 5% CO2 and 37 degrees Celsius cell incubator. Inhibitors included: 5-10 mM of 2-deoxyglucose (2-DG; in mQ water; #D8375-1g, Sigma), 20 µM ST045849 (ST; in DMSO; #6775, Tocris) and 10 µM Thiamet G (TG; in DMSO; #13237, Cayman Chemical, Ann Arbor, Michigan, United States). Antigens included 100 ng/mL of ultrapure lipopolysaccharides (LPS; *Escherichia coli* 0111 B4 strain, #tlrl-3pelps, InvivoGen), 20 µg/mL of polyinosinic:polycytidylic acid (PolyIC; high molecular weight, #TLRL-PIC, InvivoGen), 20-50 µg/mL of zymosan (#Z4250, Sigma), 250-500 ng/mL of

omega-1 (in-house), 25-50 µg/mL of soluble egg antigen (SEA; *Schistosoma mansoni* Puerto Rican strain, in-house) and 10 µg/mL of house dust mite (HDM; Greer, lot number: 305470). Supernatants were collected after 24 hours and IL-10 and IL-12p70 concentrations were determined using ELISA. Alternatively, 10.000 24h-stimulated DCs were co-cultured with 10.000 J558-CD40L cells - a CD40L-expressing cell line – for another 24 hours before determination of cytokine concentrations. Viability, differentiation markers and expression of costimulatory molecules were determined using flow cytometry on a FACSCanto II.

Analysis of blood DCs from a controlled human hookworm infection trial.
Peripheral venous blood was drawn from healthy volunteers prior to and 8 weeks after infection with *Necator americanus*, as part of a controlled human infection trial (NCT03126552) [28]. PBMCs were isolated as described above and cryopreserved in liquid nitrogen until later analysis.

Preparation of Schistosoma mansoni soluble egg antigens and omega-1
S. mansoni eggs were isolated and processed into a SEA preparation as described previously [18]. Protein concentration was determined using a bicinchoninic acid (BCA) protein assay kit (Pierce, #PIER23225). Endotoxin contamination was determined by a direct comparison of SEA batches to LPS in a TLR4-transfected Human Embryonic Kidney 293 (HEK) reporter cell line, in which IL-8 secretion by 5x10^8 HEK cells after stimulation with 10 µg of SEA is expected to be similar or less than after stimulation with 1-3 ng/mL of LPS. Omega-1 was purified from SEA as described [18].

T cell polarization
Naïve CD4 T cells for assessment of DC capacity for Th1/2 polarization were isolated from allogeneic buffy coat PBMCs using a naïve human CD4 T cell isolation kit (#480042, BioLegend). Memory CD4 T cells for assessment of DC capacity for Th17 reactivation were isolated using a human CD4 T cell isolation kit (#130-096-533, Miltenyi) followed by a combination of anti-CD45RO-PE (UCHL1 clone; #R0843, Dako) and anti-PE microbeads (#130-048-801) to eliminate naïve CD4 T cells. For Th1/2 polarization, 5.000 DCs that were stimulated for 24h were co-cultured with 20.000 allogeneic naïve CD4 T cells in the presence of 20 pg/mL Staphylococcal Enterotoxin B (SEB; #S4881, Sigma) in a cell culture treated flat-bottom 96 well plate. After 5-7 days, cells were transferred to a flat-bottom 24 well plate well containing 1 mL of media that was supplemented with 42 IU/mL recombinant human IL-2 (#202-IL, R&D systems). 2 days later, 1 mL of fresh media with IL-2 was added and cell cultures were split into two. Cells were restimulated at approximately 11 days with 100 ng/mL phorbol myristate acetate (PMA) and 2 µg/mL ionomycin for a total 6 hours, of

which the last 4 hours in the presence of 10 µg/mL brefeldin A (#B-7651, Sigma). Cells were stained with Aqua LIVE/DEAD and fixed with formalin as described in the next section before permeabilization with a permeabilization buffer (#00-8333-56, Thermo) according to the manufacturer's recommendation. Production of IL-4 and IFNγ was determined using flow cytometry. For Th17 reactivation, 2.000 stimulated DCs were co-cultured with 20.000 allogeneic memory CD4 T cells in IMDM (#12-722F, Lonza) supplemented with 10% HI-FCS, 100 U/mL penicillin and 100 µg/mL streptomycin in the presence of 10 pg/mL SEB in a flat-bottom 96 well plate. Supernatants were collected after 5 days and IL-17 concentration was determined using ELISA.

Flow cytometry

In general, single cell suspensions underwent viability staining for 20 minutes at room temperature using the LIVE/DEAD™ Fixable Aqua Dead Cell Stain Kit (#L34957, Thermo) 1:400 in PBS and fixation for 15 minutes at room temperature using 1.85% formaldehyde (F1635, Sigma) in PBS before surface staining with antibodies in a non-sterile version of the in-house cell separation buffer (=FACS buffer) for 30 minutes at 4 degrees Celsius. Alternatively, cells were acquired unfixed in FACS buffer with 7-AAD (#00-6993-50, eBioscience) 1:50 to distinguish live from dead cells. Compensation was done using single staining on beads (#552843, BD Biosciences or 552845, BD Biosciences or #A10346, Invitrogen)

For detection of protein O-GlcNAcylation in moDCs, cells underwent Aqua viability staining for 30 minutes on ice and fixation for 60 minutes at 4 degrees using the Foxp3 / Transcription Factor Staining Buffer Set (#00-5523-00, eBioscience). Afterwards, cells were further permeabilized by first resuspending them in 20 µL of ice-cold PBS and then adding 180 µL of ice-cold absolute methanol (90% end concentration; #1.06009, Merck). Methanol was added carefully to prevent leaking of methanol out of the pipette tips and overflowing of the well plates. Cells were fixed for at least 10 minutes at -20 degrees Celsius up to overnight. Methanol was washed away with FACS buffer at least two times before staining O-GlcNAcylation, CD1a and CD14 to prevent interaction with methanol sensitive fluorochromes. Cells were analyzed on a FACSCanto II.

To assess levels of O-GlcNAcylation in DCs subsets in frozen human blood, PBMCs were thawed and first live stained for the following surface markers during the fixable Aqua stain: CD3/CD56/CD19, which were used as exclusion markers, and HLA-DR and CD11c, which in combination with CD123, CD141, and CD1c were used to identify pDCs, cDC1s and cDC2s respectively. Cells were then washed in PBS and fixed with an Intracellular Fixation & Permeabilization Buffer Set (#88-8824-00, eBioscience) for 1 h at 4 degrees Celsius. Cells we washed again in PBS

and subsequently permeabilized using the same set before a second staining for O-GlcNAcylation as described above. Cells were analyzed on an LSR-II.

All samples were run on a FACSCanto II or LSR-II (both BD Biosciences) and analyzed using FlowJo (Version 10, TreeStar, Meerhout, Belgium).

Antibodies

The antibodies used in this study can be found in supplementary table 1.

RNA sequencing and metabolomics

moDCs from three 6-well plates were pooled, centrifuged and resuspended in 1 mL himRPMI. 300 µL was used for mRNA extraction, 300 µL was used for metabolite extraction, 300 µL was used for extracellular flux (XF) analysis and the remaining 100 µL was used for cell counting, analysis of DC activation and T cell polarization. Cell numbers for mRNA extraction and metabolite extraction ranged between 0.3-1.1 million cells.

mRNA was extracted with oligo-dT beads (Invitrogen) and libraries were prepared and quantified as described before [56].

Extraction of metabolites was done according to the recommendations of General Metabolomics (Boston, Massachusetts, USA) specifically for extraction of polar metabolites from adherent mammalian cell culture. Briefly, cells were transferred to 1.5 mL Eppendorfs, centrifuged, washed using a warm ammonium carbonate wash solution (75 mM ammonium carbonate [#A9516, Sigma] in HLPC-grade water and pH 7.4 titrated with HLPC-grade formic acid) and resuspended in a 70 degrees Celsius 70% ethanol extraction solvent (70% v/v absolute ethanol [#100983.1000, Merck] in HLPC-grade water). After exactly 3 minutes, the extracts were transferred to other, pre-chilled Eppendorfs in a dry-ice bed. The first group of Eppendorfs were washed with a second volume of extraction solvent that was immediately transferred to the second group of Eppendorfs. Combined extracts were then centrifuged at 14.000 rpm for 10 minutes at 4 degrees Celsius or colder, after which a fixed volume of the extract supernatant was collected – without disturbing any pelleted material – and transferred to a third group of Eppendorfs, also pre-chilled and in a dry-ice bed. The materials were stored at -80 degrees Celsius before shipping processing by General Metabolics as described in [16].

RNA-seq and metabolic network analysis

RNA-seq libraries were sequenced using paired-end sequencing, second read (read-mate) was used for sample demultiplexing. Reads were aligned to the GRCh37 assembly of human genome using STAR aligner. Aligned reads were quantified using quant3p script (https://github.com/ctlab/quant3p) to account

for specifics of 3' sequencing with protein-coding subset of Gencode gene annotation. DESeq2 was used for differential expression analysis. Metabolic network clustering analysis was done with GAM-clustering method [57] based on gene expression profiles and metabolic network based on KEGG database. Metabolic module for Th2-DC vs iDC comparison was done using GATOM method as described in Ulland et al. [58] based on both DESeq2-based differential expression results for genes and limma-based differential analysis results for metabolites.

Extracellular flux analysis

For real-time metabolic analysis on live cell, DCs were resuspended in Seahorse media (= unbuffered RPMI [#R1383-10X1L, Sigma] of which the pH was set to 7.4 using 37% HCl (#1.00317.1000, Merck) before sterilization using a 0.22 µm filter system that was supplemented with 5% HI-FCS and plated in XF cell culture plates (part of pack #102416-100, Agilent, Amstelveen, The Netherlands) at 5x10^4 cells per 180 µL of Seahorse media. The plate was quickly spun down to facilitate the adherence of cells to the bottom of the well and then, the cells were rested for 1 hour in a special 0% CO_2 cell incubator at 37 degrees Celsius. This rest time is also needed for the evaporation of remaining CO_2 in the media, which can acidify the unbuffered media. To facilitate the adherence of semi-adherent DCs even more, the assay plate wells were coated beforehand with 25 µL of 50 µg/mL Poly-D-Lysine hydrobromide (PDL; diluted in mQ water; # A-003-E, Merck) for a minimum of 1 hour at 37 degrees Celsius, after which the PDL was pipetted away and the wells were washed using 200 µL of mQ water and subsequent air-drying. MilliQ water is preferred over PBS here as air-drying PBS residues might result in crystal formation. During the rest, pre-hydrated XF cartridges were filled with 10x concentrated assay reagents in Seahorse media that did not contain HI-FCS for sequential injections of glucose (10 mM end; port A; #G8644-100mL, Sigma), oligomycin (1 µM end; port B; #11342, Cayman Chemical), fluoro-carbonyl cyanide phenylhydrazone (FCCP, 3 µM end; port C; # C2920-10MG, Sigma), and finally, rotenone/antimycin A (1/1 µM end; port D; #R8875-1G/#A8674-25MG, Sigma). The manufacturer recommended the removal of HI-FCS from the injection solution to prevent clogging of the injection ports. Oxygen consumption rates (OCR) and extracellular acidification rates (ECAR) were recorded with the XF96e Extracellular Flux analyser (Agilent) and analyzed using Wave Desktop (Version 2.6, Agilent). Immediately after the run, XF culture plates were collected from the analyser, supernatants were carefully pipetted away, cells were washed gently with PBS, lysed in 25 µL of a RIPA-like buffer (50 mM Tris-HCl [pH 7.4], 150 mM NaCl and 0.5% SDS) and the plate was stored at -20 degrees Celsius for later protein content quantification using bicinchoninic acid protein assay kit (BCA; #PIER23225, Pierce) according to the manufacturer's recommendations.

Glycolytic rate = increase in ECAR in response to injection A. Glycolytic capacity = increase in ECAR in response to injection A and injection B. Baseline OCR = difference in OCR between readings following port A injection and readings after port D injection. Spare OCR is difference between basal and maximum OCR, which is calculated based on the difference in OCR between readings following port C injection and readings after port A injection. ATP production = difference in OCR between readings following port A injection and readings after port B injection. Proton leak = difference in OCR between readings following port B injection and after port D injection. A more detailed description of this procedure can be found somewhere else [59].

Western blotting

DCs were washed twice with PBS before being lysed in EBSB buffer (8% [w/v] glycerol, 3% [w/v] SDS and 100 mM Tris–HCl [pH 6.8]). Lysates were immediately boiled for 5 min and their protein content was determined using a BCA kit. Protein was separated by SDS-PAGE followed by transfer to a PVDF membrane. Protein content of 1 million moDCs that were stimulated for 24h but not recounted before lysis in 150 µL was approximately 0.5 mg/mL. Usually 10 µg of protein was added to each lane. Membranes were blocked for 1 h at room temperature in TTBS buffer (20 mM Tris-HCl [pH 7.6], 137 mM NaCl, and 0.25% [v/v] Tween 20) containing 5% (w/v) fat free milk and incubated overnight with primary antibodies. The primary antibodies used were O-GlcNAc (RL2 clone; 1:1000, #?, company?), OGT (D1D8Q clone; 1:1000; #24083S, Cell Signaling and beta-actin (AC-15 clone; 1:10.000; #A5441, Sigma). The membranes were then washed in TTBS buffer and incubated with horseradish peroxidase-conjugated secondary antibodies for 2 h at room temperature. After washing, blots were developed using enhanced chemiluminescence.

qPCR

RNA was extracted from snap-frozen pulsed DCs. The isolation of mRNA was performed according to manufacturer's instruction using micro RNA Plus kit (Qiagen). cDNA was synthesized with reverse transcriptase kit (Promega) and PCR amplification by the SYBER Green method were done using CFX (Biorad). Specific primers for detected genes are as follows: human OGT forward is AGAAGGGCAGTGTTGCTGAAG and reverse is TGATATTGGCTAGGTTATTCAGAGAGTCT. The cycle threshold (Ct) value is defined as the number of PCR cycles in which the fluorescence signal exceeds the detection threshold value. The normalized amount of targeted mRNA (Nt) was calculated from Ct value obtained for both target and ACTB mRNA (served as housekeeping gene) with the equation Nt=2Ct(β-actin)-Ct(target). Relative mRNA expression was obtained by setting Nt in control as 1 in each experiment and for each donor.

Quantification and statistical analysis

Statistical analysis as specified in figure legends were performed with Prism 9 (GraphPad software Inc.). Graphs with 2 bars were analyzed with the paired Student's t test, while graphs with more than 2 bars were analyzed with the repeated measures analysis of variance (ANOVA) corrected for multiple comparisons using Sidak's multiple comparison test. A p value < 0.05 was considered significant (* for $p < 0.05$, ** for $p < 0.01$ and *** for $p < 0.001$).

Acknowledgements

This work was supported by an LUMC fellowship and a VENI grant (#91614087 by Netherlands Organisation for Scientific Research) awarded to BE.

Author contributions

LP, MQ, AvdH, LB and BW performed experiments. LP, AS and BE analyzed experiments. GS provided omega-1. MR provided PBMCs from the controlled human hookworm infection trial. LP, CH, MA and BE designed experiments. BE conceived and supervised the study and wrote the manuscript together with LP.

Conflict of interest

The authors declare that no competing financial interests exist in relation to the work described.

Supplemental figures

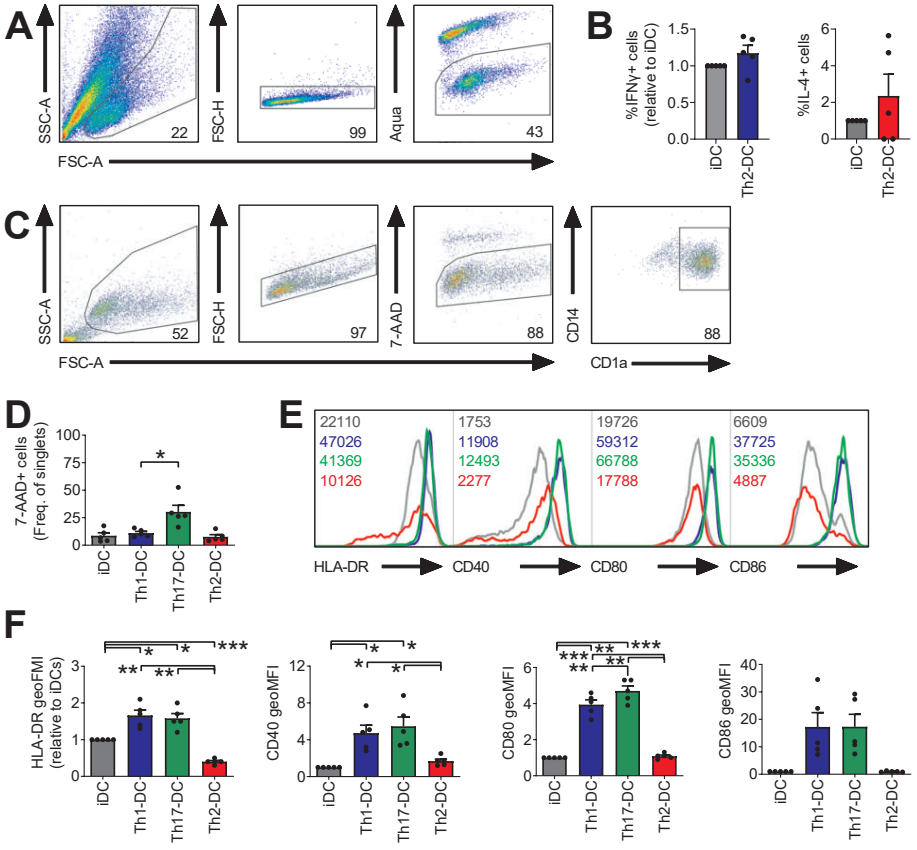

Figure S1.

Human moDCs were left untreated (iDC in grey) or stimulated for 24h with either LPS+PolyIC (Th1-DC in dark blue), zymosan (Th17-DC in green) or omega-1 (Th2-DC in red). DCs were then set aside for determination of viability (D) and maturation (E-F) using flow cytometry (C). If DC quality was sufficient, they were furthermore co-cultured with allogeneic naïve T cells for 11 days. T cell cytokine production was assessed using intracellular cytokine staining (B) using flow cytometry (A).

(A) Flow gating strategy for live T cells in 11-day old cultures of DCs and T cells by sequential gating for lymphocytes, singlets and live cells.

(B) The percentages of T cells uniquely positive for either IFNγ or IL-4 are expressed relative to the iDC condition.

(C) Flow gating strategy for live differentiated DCs by sequential gating for myeloid cells, singlets, live cells and CD1a+CD14intermediate cells after 6 days of differentiation - in the presence of GM-CSF and IL-4 - followed by 24 hours of stimulation with antigens.

(D) Frequencies of dead DCs are enumerated.

(E-F) The expression of maturation makers – based on the geometric mean fluorescence

– are shown in representative histograms with representative absolute values in E) and enumerated relative to iDCs in F).
The number of independent experiments is represented by symbols in the graphs and shown as mean ± SEM; *p < 0.05, **p < 0.01, ***p < 0.001

A

Gene set enrichtment analysis
on genes in metabolic cluster 3 using pathways supplied by the Kegg database

Gene set description	# genes in overlap (k)	FDR q-value
Glycolysis / Gluconeogenesis	8	2.18 e^{-13}
Terpenoid backbone biosynthesis	6	2.5 e^{-13}
Steroid biosynthesis	6	4.11 e^{-13}
Valine, leucine and isoleucine degradation	7	7.75 e^{-13}
Pyruvate metabolism	6	7.52 e^{-11}
Fatty acid metabolism	5	1.63 e^{-8}
Peroxisome	5	3.39 e^{-7}
Propanoate metabolism	4	6.81 e^{-7}
Glutathione metabolism	4	3.37 e^{-6}
Biosynthesis of unsaturated fatty acids	3	2.32 e^{-5}

B

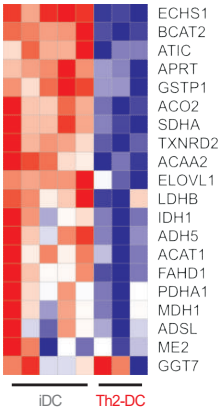

C

Gene set enrichtment analysis
on genes in metabolic cluster 8 using pathways supplied by the Kegg database

Gene set description	# genes in overlap (k)	FDR q-value
Citrate cycle (TCA cycle)	6	6.94 e^{-13}
Pyruvate metabolism	5	7.22 e^{-10}
Fatty acid metabolism	4	2.01 e^{-7}
Valine, leucine and isoleucine degradation	4	2.01 e^{-7}
Gloxylate and dicarboxylate metabolism	3	1.71 e^{-6}
Propanoate metabolism	3	1.3 e^{-5}
Butanoate metabolism	3	1.3 e^{-5}
Glutathione metabolism	3	3.7 e^{-5}
Glycolysis / Gluconeogenesis	3	6.32 e^{-5}
Valine, leucine and isoleucine biosynthesis	2	2.04 e^{-4}

Figure S2.

Human moDCs were left untreated (iDC in grey) or stimulated for 24h with either LPS+PolyIC (Th1-DC in dark blue), zymosan (Th17-DC in green) or omega-1 (Th2-DC in red). DCs were then set aside for RNA-sequencing. Metabolic genes were selected out of the total transcriptome of differently conditioned DCs and used to form 13 clusters with maximal distinguishing power. Pathway analysis was done on the genes in these metabolic clusters. Top pathways in cluster 3 (A) and 8 (C) are shown here, as well as an overview of genes in metabolic cluster 8 (B).
The number of independent experiments is represented by blocks in the heat map.

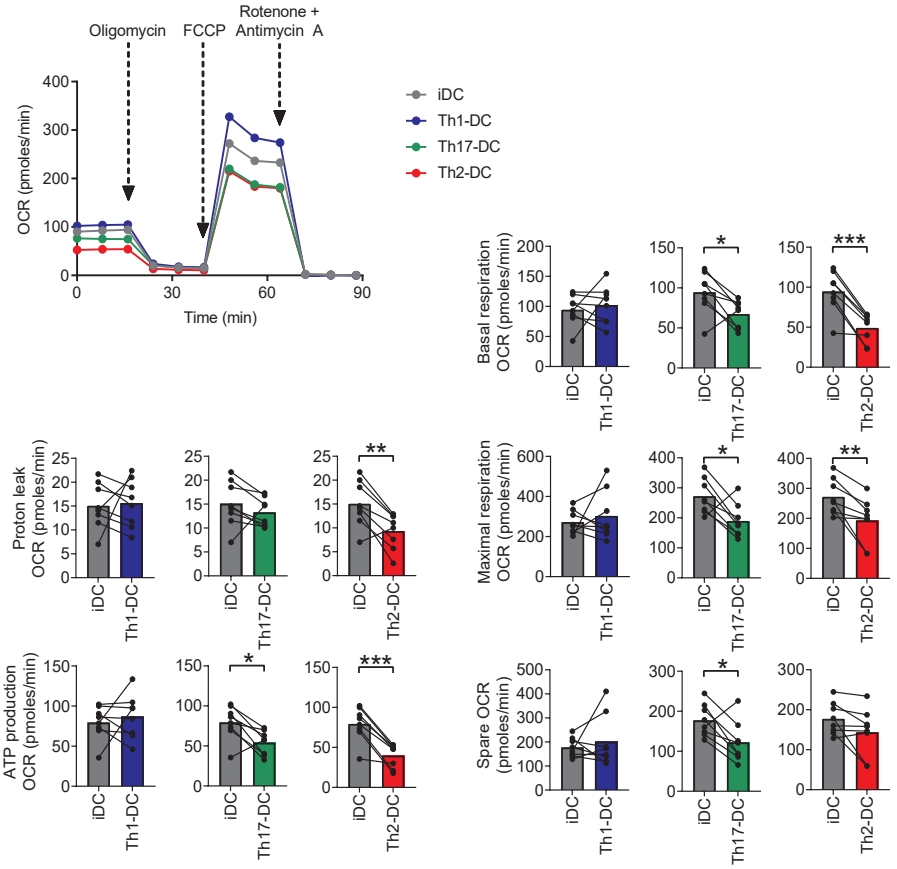

Figure S3.

Human moDCs were left untreated (iDC in grey) or stimulated for 24h with either LPS+PolyIC (Th1-DC in dark blue), zymosan (Th17-DC in green) or omega-1 (Th2-DC in red). DCs were then set aside for measurements of mitochondrial respiration using extracellular flux (XF) analysis.

Mitochondrial stress test in Seahorse XF analyzer which consists of sequential injections of oligomycin, FCCP and Rotenone + Antimycin A. Measurements of mitochondrial respiration were determined after subtraction of non-mitochondrial oxygen consumption = oxygen consumption rate (OCR) after injection of Rotenone + Antimycin A Basal respiration = OCR before injection of oligomycin. Max respiration = OCR after injection of FCCP. Spare OCR = difference basal and max respiration. Proton leak = OCR after injection of oligomycin. (Mitochondrial) ATP production = the difference before and after injection of oligomycin.

The number of independent experiments is represented by symbols in the graphs and shown as mean ± SEM; *p < 0.05, **p < 0.01, ***p < 0.001

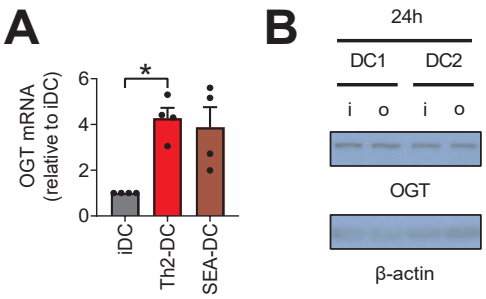

Figure S4.

Human moDCs were left untreated (iDC in grey / i) or stimulated for 24h with either omega-1 (Th2-DC in red / o) or *Schistosoma mansoni* soluble egg antigens (SEA-DC). DCs were then set aside for qPCR (A) or western blotting (B).
(A) Proteins were visualized by western blotting using antibodies against O-GlcNAc transferase (OGT) and beta-actin. Beta-actin was taken along as housekeeping protein.
(B) The mRNA expression of OGT was determined.
The number of independent experiments is represented by symbols in the graphs and shown as mean ± SEM; *p < 0.05

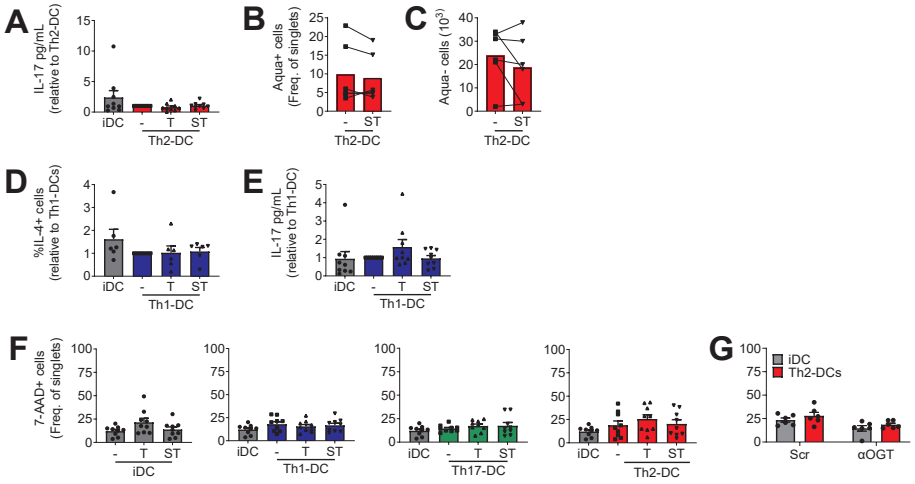

Figure S5.

Human moDCs were differentiated as normally (A-F) or short interfering RNA was introduced against O-GlcNAc transferase (OGT) at day 4 (G). Scrambled RNA was used as a control. At day 6, DCs were stimulated as normal with either LPS+PolyIC (Th1-DC in dark blue), zymosan (Th17-DC in green), omega-1 (Th2-DC in red) for 24 hours or left untreated (iDC in grey). DCs were then set aside for co-culture with allogeneic T cells (A-E) or viability was determined using flow cytometry (F-G).
(A, E) Co-culture with memory T cells. Supernatants were collected after 5 days and IL-17 concentrations was determined by ELISA.
(B-D) Co-culture with naïve T cells for 11 days. T cell viability (B) and numbers (C) were determined using flow cytometry. T cell intracellular IFNγ and IL-4 was analyzed by flow cytometry after a 6h stimulation with phorbol myristate acetate (PMA) and ionomycin (D). The percentages of T cells uniquely positive for either IL-4 are expressed relatively.
(F-G) Frequencies of dead DCs are enumerated.
The number of independent experiments is represented by symbols in the graphs and shown as mean ± SEM.

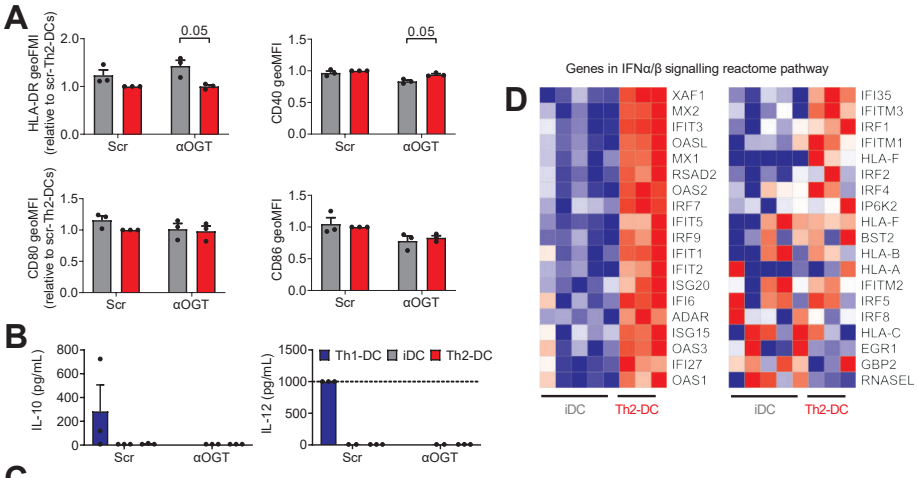

C

Reactome pathway analysis on top 200 DEGs up in Th2-DCs vs iDCs

Index	Name	Adjusted p-value	Combined score
1	Interferon alpha/beta signaling	1.25E-13	801.78
2	Interferon Signaling	5.04E-15	472.38
3	TRAIL signaling Homo sapiens	0.006402	441.63
4	CASP8 activity is inhibited	0.02344	239.56
5	Regulation by c-FLIP	0.02131	239.56
6	Dimerization of procaspase-8	0.01953	239.56
7	NF-kB activation through FADD/RIP-1 pathw ay mediated by caspase-8 and -10	0.02386	212.59
8	ISG15 antiviral mechanism	0.00001262	212.54
9	Antiviral mechanism by IFN-stimulated genes	0.00001052	212.54
10	Interferon gamma signaling	0.000012	185.78

Figure S6.

Human moDCs were differentiated as normally (C) or short interfering RNA was introduced against O-GlcNAc transferase (OGT) at day 4 (A-B). Scrambled RNA was used as a control. At day 6, DCs were stimulated as normal with omega-1 (Th2-DC in red) for 24 hours or left untreated (iDC in grey). Supernatants were then collected for determination of IL-10 and IL-12p70 secretion (B) and DCs were set aside for RNA-sequencing (C) and determination of maturation (A).
(A) The expression of maturation makers – based on the geometric mean fluorescence – are shown relative to iDCs.
(B) IL-10 and IL-12p70 concentrations was determined by ELISA.
(C) Top pathways are shown of pathway analysis on total transcriptome of differently conditioned DCs.
The number of independent experiments is represented by symbols in the graphs and shown as mean ± SEM.

Supplementary tables

Table 1. Antibodies used in study.

Target	Clone	Conjugate	Source	Identifier	Dilution
IL-4	8D4-8	PE	BD Biosciences	554516	1:250
IFNγ	25723.11	FITC	BD Biosciences	340449	1:20
CD16/32	Polyclonal	Pure	eBiosciences	14-9161	1:100
CD1a	BL6	PE	Beckman Coulter	A07742	1:50
CD14	MφP9	PerCP	BD Biosciences	345786	1:50
CD86	2331	PE-Cy7	BD Biosciences	561128	1:120
CD40	5C3	APC	BD Biosciences	555591	1:50
HLA-DR	LN3	APC-eF780	eBiosciences	47-9956	1:250
CD80	L307.4	HV450	BD Biosciences	560442	1:1000
O-GlcNAc	RL2	APC	Novus	NB300-524APC	1:4000
HLA-DR	G46-6	BV605	BD Biosciences	562844	1:50
CD1c	L161	BV711	BioLegend	331535	1:100
CD141	M80	BV421	BioLegend	344113	1:800
CD11c	B-ly6	PE-Cy7	BD Biosciences	561356	1:300
CD123	7G3	FITC	BD Biosciences	558663	1:50
CD56	B159	PE	BD Biosciences	555516	1:50
CD19	HIB19	PE	BioLegend	302207	1:100
CD3	UCHT1	PE	BioLegend	300407	1:50